

# A Statistical Study of Resistive Switching Parameters in Au/Ta/ZrO<sub>2</sub>(Y)/Ta<sub>2</sub>O<sub>5</sub>/TiN/Ti Memristive Devices

David Maldonado, Alexey I. Belov, Maria N. Koryazhkina, Francisco Jiménez-Molinos, Alexey N. Mikhaylov, and Juan B. Roldán\*

Variability is an inherent property of memristive devices based on the switching of resistance in a simple metal–oxide–metal structure compatible with the standard complementary metal–oxide–semiconductor fabrication process. For each specific structure, the variability should be measured and assessed as both the negative and positive factors for different applications of memristive devices. In this report, it is shown how this variability can be extracted and analyzed for such main parameters of resistive switching as the set and reset voltages/currents and how it depends on the methodology used and experimental conditions. The obtained results should be taken into account in the design and predictive simulation of memristive devices and circuits.

## 1. Introduction

In recent years, memristive devices and crossbar arrays have been considered as the main electronic components for many artificial intelligence applications.<sup>[1]</sup> Most of these applications are based on the ability of memristive devices to adaptively change the conductivity (resistive state) depending on the history of electrical stimulation.<sup>[2,3]</sup> This ability makes it possible to mimic synaptic behavior and provides a natural colocation of information storage and processing, which improves by orders of magnitude

such main parameters of artificial neural networks (ANNs), as energy efficiency and computational throughput.<sup>[3,4]</sup>

Although different memory technologies are being developed based on various physical mechanisms (magnetic, ferroelectric, phase transition, etc.) responsible for the change in resistance, the redox-based resistive random access memory, in the form of metal–oxide–metal devices is superior in terms of switching speed, endurance,<sup>[5]</sup> retention, and number of states and differs by the simplest structure, scalability, and compatibility with the standard complementary metal–oxide–semiconductor


fabrication process.<sup>[6]</sup> A feature of such memristive devices is the variability of switching parameters both from device to device (D2D) and from cycle to cycle (C2C).<sup>[7,8]</sup> Although this feature of memristive devices is very critical from the viewpoint of traditional ANN architectures, when the reproducible and reprogrammable change of memristor states is required (e.g., for the ANN weight coefficients), much greater prospects are associated with new brain-like architectures (e.g., spiking neural networks). Such architectures can rely on the rich dynamics of memristive devices and the self-organization of plastic memristive connections.<sup>[9]</sup> Their similarity to the living brain architectures will make it possible to take the next step towards the hybrid intelligence based on the symbiosis of electronic and biological subsystems.<sup>[10,11]</sup> In addition, there are many other applications, including stochastic computing and probabilistic networks, as well as hardware information security primitives,<sup>[12–14]</sup> in which memristive devices act as the sources of randomness and entropy.

The mentioned applications require, on the one hand, strictly taking into account the variability as an undesirable and destabilizing factor when designing functional circuits based on memristors<sup>[15–17]</sup> and, on the other hand, statistically correct determination and analysis of variability for the predictive simulation of large-scale arrays of stochastic memristive devices, subsequent design, and implementation of memristive circuits. An efficient application of this approach was recently demonstrated<sup>[18]</sup> with the aim to develop a computationally lightweight model of the large array of solid-state synapses. For this purpose, the extraction of the resistive switching (RS) main parameters was carried out based on the real-world statistical data for individual HfO<sub>2</sub>-based resistive memory cells. Various methods can be used to automatically determine such parameters from long-time series mainly to analyze and correctly reproduce the C2C variability.<sup>[19–23]</sup> At the same time, the result significantly

D. Maldonado, F. Jiménez-Molinos, J. B. Roldán  
Departamento de Electrónica y Tecnología de Computadores  
Facultad de Ciencias Universidad de Granada  
Avd. Fuentenueva s/n, 18071 Granada, Spain  
E-mail: jroldan@ugr.es

A. I. Belov, M. N. Koryazhkina, A. N. Mikhaylov  
Laboratory of Stochastic Multistable Systems  
Lobachevsky State University of Nizhny Novgorod  
23/3 Gagarin Avenue, 603022 Nizhny Novgorod, Russia

A. I. Belov, M. N. Koryazhkina, A. N. Mikhaylov  
Laboratory of Intellectual Neuromorphic Systems  
Lobachevsky State University of Nizhny Novgorod  
23/3 Gagarin Avenue, 603022 Nizhny Novgorod, Russia

 The ORCID identification number(s) for the author(s) of this article can be found under <https://doi.org/10.1002/pssa.202200520>.

© 2022 The Authors. *physica status solidi (a)* applications and materials science published by Wiley-VCH GmbH. This is an open access article under the terms of the Creative Commons Attribution-NonCommercial License, which permits use, distribution and reproduction in any medium, provided the original work is properly cited and is not used for commercial purposes.

DOI: 10.1002/pssa.202200520

depends not only on the extraction method used, but also on the measurement conditions and the fabrication technology of memristive devices. Therefore, it is a very relevant problem to develop and test new numerical methods for extraction, modeling, and prediction of variability on specific memristive devices.

In this work, these methods are tested on the example of previously engineered Au/Ta/ZrO<sub>2</sub>(Y)/Ta<sub>2</sub>O<sub>5</sub>/TiN/Ti memristive devices, which demonstrate reproducible bipolar-type RS.<sup>[24]</sup> Such devices exhibit stabilization of resistive states after several hundred switching cycles following the electroforming procedure. High enough endurance<sup>[5]</sup> makes it possible to investigate the influence of measurement conditions for both the same and different devices on a chip.

## 2. Device Fabrication and Measurement Setup

Memristive device under study (Figure 1a) was fabricated on top of a commercial SiO<sub>2</sub> (500 nm)/Si substrate covered by the bottom electrode TiN (25 nm)/Ti (20 nm) layers deposited by magnetron sputtering from a high-purity Ti target. The Ta<sub>2</sub>O<sub>5</sub> (10 nm) and ZrO<sub>2</sub>(Y) (10 nm) layers were deposited by radio frequency magnetron sputtering from Ta and ZrO<sub>2</sub> (12% Y<sub>2</sub>O<sub>3</sub>) targets, respectively, in the mixed Ar (50%) and O<sub>2</sub> (50%) atmosphere at the substrate temperature of 300 °C. The top electrode layers of Ta (8 nm) and Au (40 nm) were deposited by direct-current magnetron sputtering from high-purity metal targets in Ar atmosphere at the substrate temperature of 200 °C. According to previous report,<sup>[24]</sup> this combination of materials and deposition parameters provides robust RS due to the presence of grain boundaries in ZrO<sub>2</sub>(Y) serving as the preferred sites for conductive filament (CF) nucleation, self-assembled nanoclusters (NCs) in the Ta<sub>2</sub>O<sub>5</sub> film serving as the electric field concentrators, and oxygen exchange between the TaO<sub>x</sub>, ZrO<sub>2</sub>(Y) layers and interface with the bottom TiN electrode (TiO<sub>x</sub>). The experiments were performed with independent crosspoint devices with active areas of 20 μm × 20 μm. Current compliance of 300 μA was provided by a simple field-effect transistor circuit.<sup>[24]</sup>

The DC *I*-*V* curves of the memristive device (Figure 1b) were measured in a voltage sweeping mode at a sweep rate of 7.25 V s<sup>-1</sup> using an Agilent B1500A semiconductor device

parameter analyzer. The 970 consecutive set/reset cycles in RS series were obtained after electroforming and at least 300 DC sweeps required for switching stabilization.<sup>[24]</sup> The electrical contacts to the contact pads of memristive devices were provided using the EverBeig EB-6 probe station. The sign of voltage across memristive devices corresponded to the potential of top electrode relative to the potential of bottom electrode.

To study the dependence of RS parameters on the sweep rate, the current response of memristive device was registered using the voltage drop across the in-series connected resistor of 100 Ω. NI USB 6211 multifunction I/O device was used in this experiment. Ramped input voltages corresponding to different sweep rates and cycling frequencies are shown in Figure 2. These input signals were applied to a memristive device to obtain the current response time series shown in Figure 3.

## 3. Results

In this section, we will deal with the definition and application of robust extraction procedures to extract the RS parameters, such

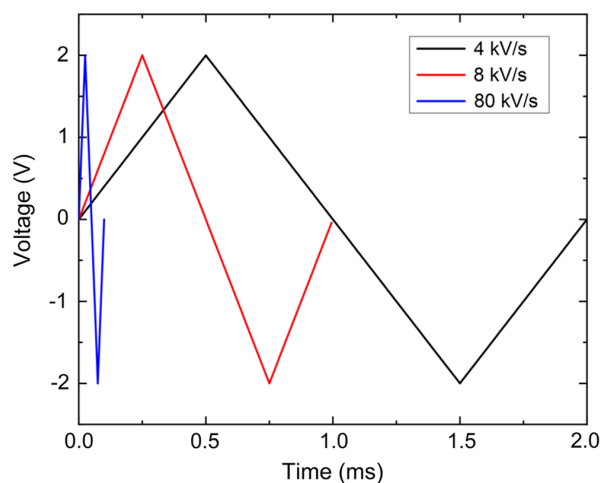


**Figure 2.** Ramped voltages used as input signals for the sweep-rate experiment. The ramp rates used were 4, 8, and 80 kV s<sup>-1</sup>.

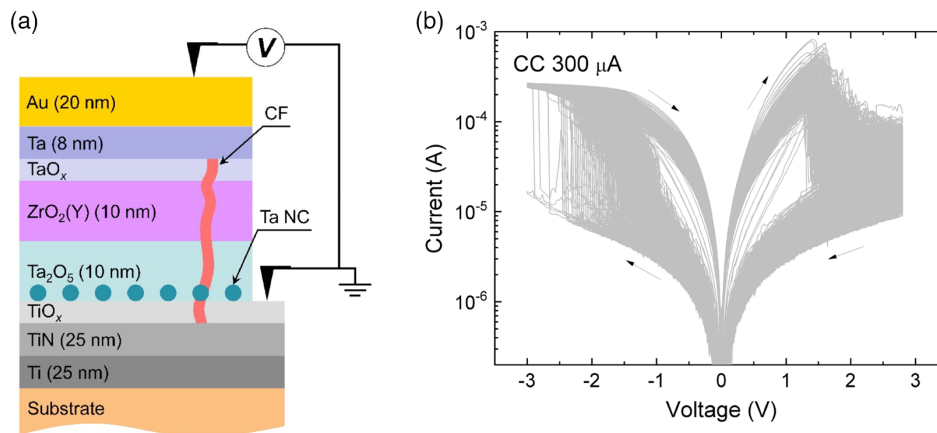


**Figure 1.** a) Schematic representation of memristive device and b) experimental *I*-*V* curves for the 970 set/reset cycles measured.

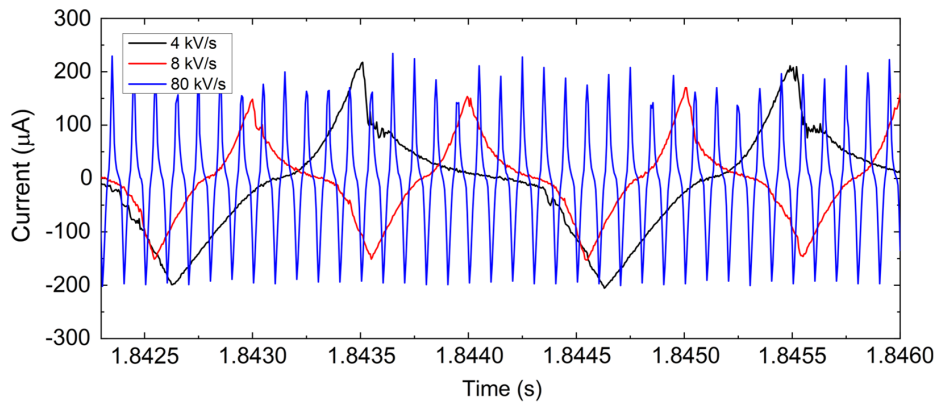


**Figure 3.** Experimental  $I-t$  measurements for the three ramp rates used and zoomed in detail.

as voltages for set and reset processes ( $V_{\text{set}}$  and  $V_{\text{reset}}$ , respectively) and the corresponding currents ( $I_{\text{set}}$  and  $I_{\text{reset}}$ ) for the devices under study.<sup>[25,26]</sup> In that respect, it is key to explain the numerical techniques used in device characterization.

### 3.1. Set Voltage Extraction Methods

The first methodology presented to extract  $V_{\text{set}}$  (MS1) relies on the detection of the maximum value of the first current derivative, as shown in **Figure 4a**. Sometimes, as a consequence of typical RS associated current fluctuations due to the device inherent stochastic behavior, this method could give rise to error. To overcome this issue, we limited the voltage range where the method is employed in the [0.6, 2.1 V] voltage interval. The second technique (MS2), adapted from the study by Maldonado et al.,<sup>[27]</sup> consists of finding the maximum separation from a theoretical straight line that connects the first point of the  $I-V$  curve measured at  $V = 0$  V and the first point where the compliance current is reached, that is, the detection of the curve knee, as shown in **Figure 4b**.

### 3.2. Reset Voltage Extraction Methods

Here we consider three different methods to extract  $V_{\text{reset}}$ . The first procedure (MR1) is based on the calculation of the first

derivative of the current, as shown in **Figure 5a**. The derivative minimum value is evaluated at the [0.6, 2.1 V] voltage interval. The second procedure (MR2) consists of finding the maximum current value along the curve, as shown in **Figure 5b**. The third technique (MR3) detects the first point where the current is decreased, making use of the first negative current derivative value, as shown in **Figure 5c**. The three methods are plotted together as depicted in **Figure 5d** leading to different  $V_{\text{reset}}$  for the same curve.

### 3.3. Results for the DC RS Series

The experimental values of the  $V_{\text{set}}$  and  $I_{\text{set}}$  for the 970 cycles analyzed, obtained using the MS1 and MS2 methods presented above, are shown in **Figure 6**. These representations allow one to evaluate the time series evolution and the autocorrelation dependencies of the data along the RS series.

The corresponding experimental voltages and currents extracted for the reset process using the three techniques proposed MR1, MR2, and MR3 are presented in **Figure 7**.

In order to compare the different results obtained for the set and reset processes using the proposed methodologies, in **Figure 8a**, the  $I_{\text{set}}$  versus  $V_{\text{set}}$  points for MS1 and MS2 are plotted. As it could be observed, the spreading for the latter method is lower. In the same way, in **Figure 8b**, the  $I_{\text{reset}}$  versus  $V_{\text{reset}}$  points

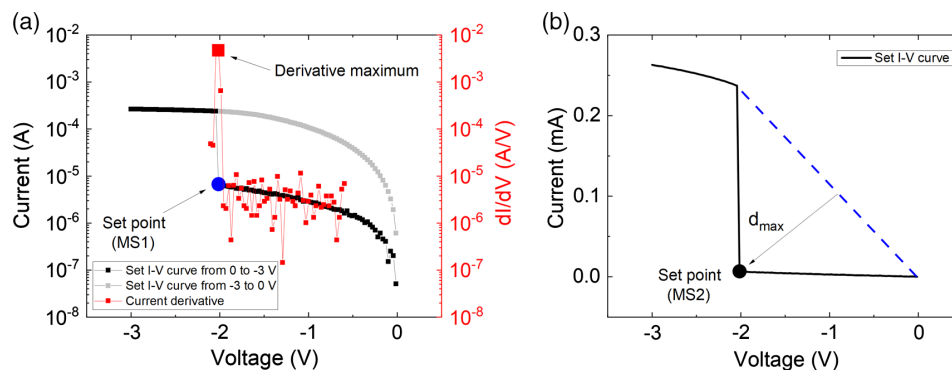


**Figure 4.** a) Experimental  $I_{\text{set}}$  (black symbols) and first current derivative (red symbols) versus voltage. The set point (using the MS1 method) is established (blue point) at the current derivative maximum. b) Experimental  $I_{\text{set}}$  (black line) versus voltage. This methodology uses a straight line (dashed) to join the first point of the experimental curve and the first one where the compliance current is reached. The maximum distance marks the  $V_{\text{set}}$  (using the MS2 method).

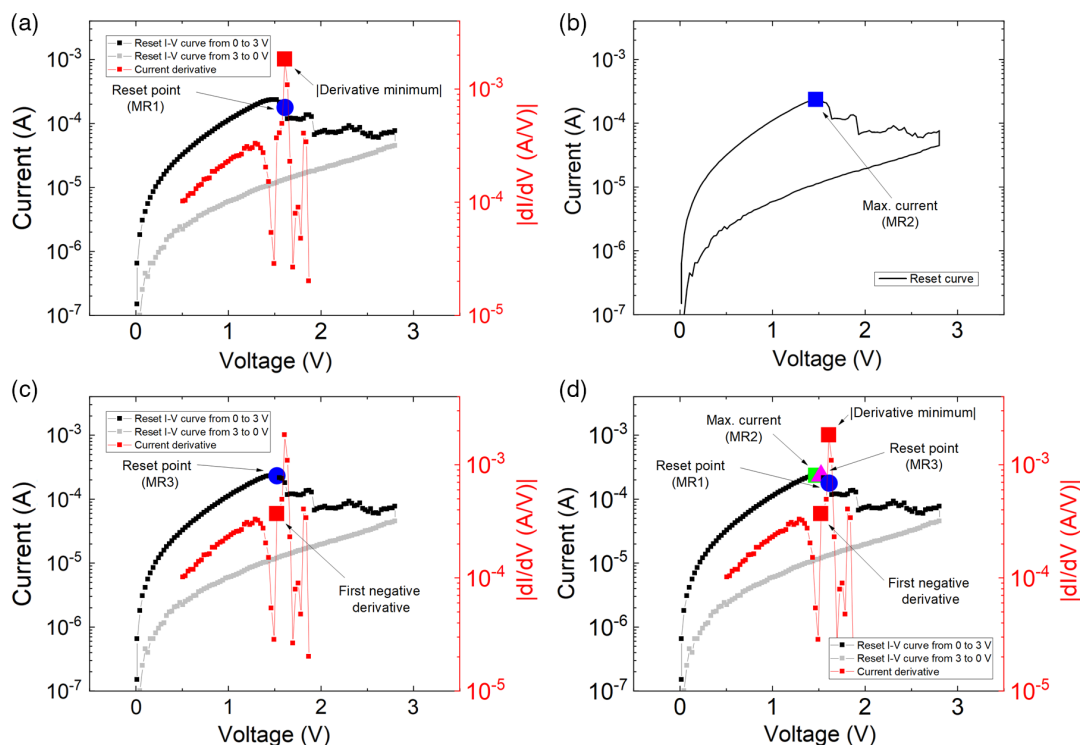


**Figure 5.** a) Experimental  $I_{\text{reset}}$  (black symbols) and first current derivative (red symbols) versus voltage. The reset point (using the MR1 method) is established by determining the minimum current derivative. b) Experimental  $I_{\text{reset}}$  versus voltage. The maximum current value is established as the reset point (using the MR2 method). c) Experimental  $I_{\text{reset}}$  (black symbols) and first current derivative (red symbols) versus voltage. The first negative derivative value is established as the reset point (using the MR3 method). d) Experimental  $I_{\text{reset}}$  (black symbols) and first current derivative (red symbols) versus voltage. The results of the  $V_{\text{reset}}$  extraction methods MR1, MR2, and MR3 are plotted together for a better visualization.

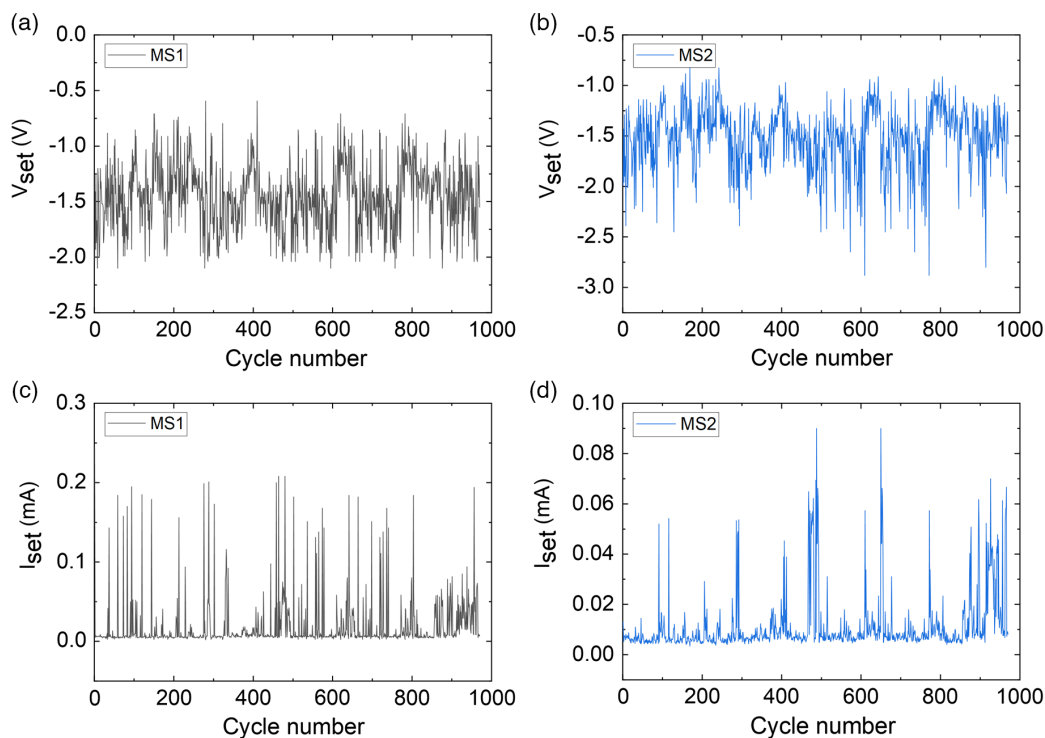


**Figure 6.** Experimental  $V_{\text{set}}$  by means of a) MS1, b) MS2 methods; and corresponding  $I_{\text{set}}$  by means of c) MS1, d) MS2 methods, versus cycle number obtained for the RS series described above.

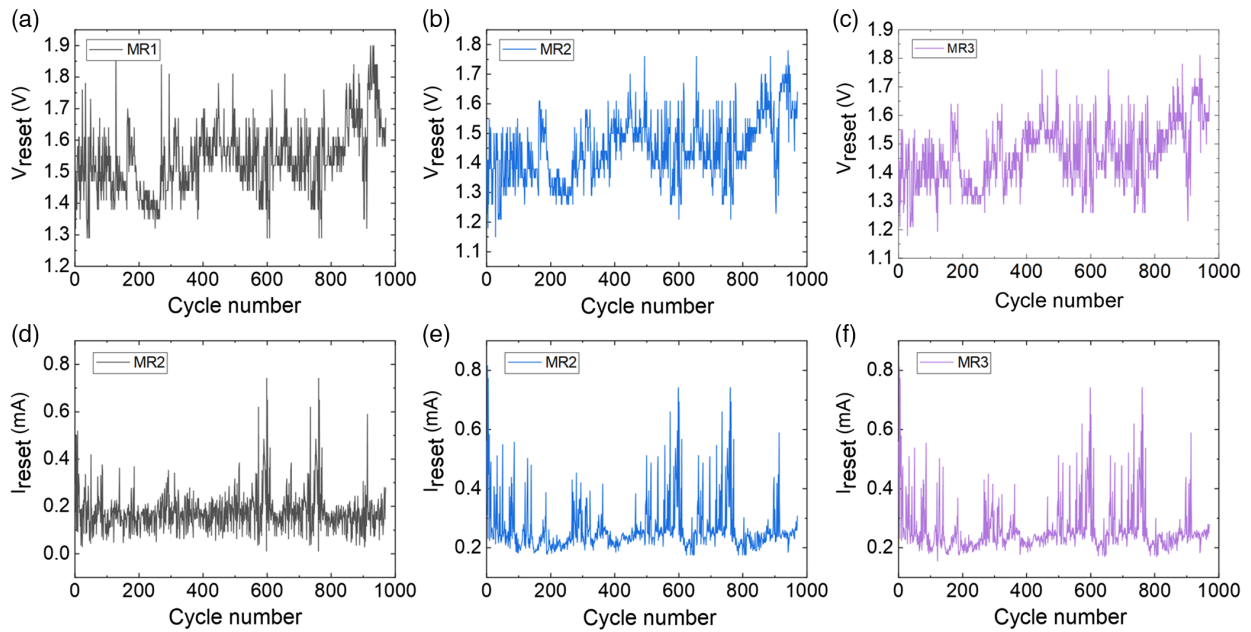


**Figure 7.** Experimental  $V_{\text{reset}}$  extracted using the a) MR1, b) MR2, c) MR3 methods; and corresponding  $I_{\text{reset}}$  for d) MR1, e) MR2, f) MR3 methods, versus cycle number obtained RS series analyzed here.

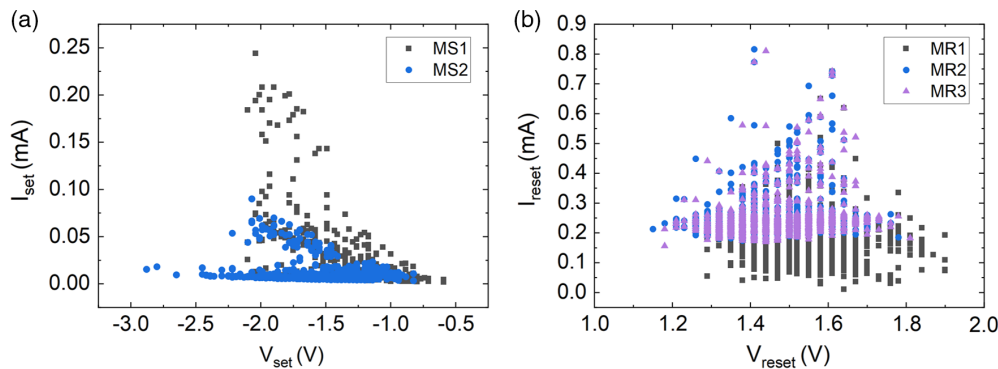


**Figure 8.** a) Experimental  $I_{\text{set}}$  versus  $V_{\text{set}}$  for the cycles analyzed by the MS1 and MS2 methods. b) Experimental  $I_{\text{reset}}$  versus  $V_{\text{reset}}$  for the cycles analyzed by the MR1, MR2, and MR3 methods.

for MR1, MR2, and MR3 are plotted together denoting that the current derivative method (MR1) presents a higher dispersion as a consequence of the measurement noise of the  $I$ - $V$  curve.

The cumulative distribution functions (CDFs) for the methods reported above are shown for  $V_{\text{set}}$  (Figure 9a),  $I_{\text{set}}$  (Figure 9b),  $V_{\text{reset}}$  (Figure 9c), and  $I_{\text{reset}}$  (Figure 9d). In particular, for the set case, the derivative determination (MS1) and the curve knee method (MS2) produce quite similar results. The same tendency is observed for the maximum current determination (MR2) and the first point with decreasing current (MR3) applied in reset case. Nevertheless, the derivative determination (MR1) clearly presents higher  $V_{\text{reset}}$  and lower  $I_{\text{reset}}$ .

In Figure 10a, the calculated Weibits for the  $V_{\text{set}}$  are plotted resulting in a straight line for the curve knee method (MS2) which demonstrates that the  $V_{\text{set}}$  obtained using this method follows the Weibull distribution (it is not the case for MS1). This

situation, as shown in Figure 10b, does not apply for the  $V_{\text{reset}}$  in any presented methods.

### 3.4. Results for the RS Series at Fast Ramp Rates

Every single  $I$ - $t$  measurement shown in Figure 3 was used to plot  $I$ - $V$  curves by adding its corresponding ramped voltage (obtained from Figure 2). In order to show the shape of the curves for the sake of clarity, some individual cycles are presented in Figure 11 for the ramp rate of  $4 \text{ kV s}^{-1}$ , Figure 12 for  $8 \text{ kV s}^{-1}$ , and Figure 13 for  $80 \text{ kV s}^{-1}$ . The method to determine the reset voltage consists of finding the current maximum and the set voltage is found by obtaining the current minimum (in the analysis absolute values are considered). Thus, the black (red) dots mark the reset (set) voltages.

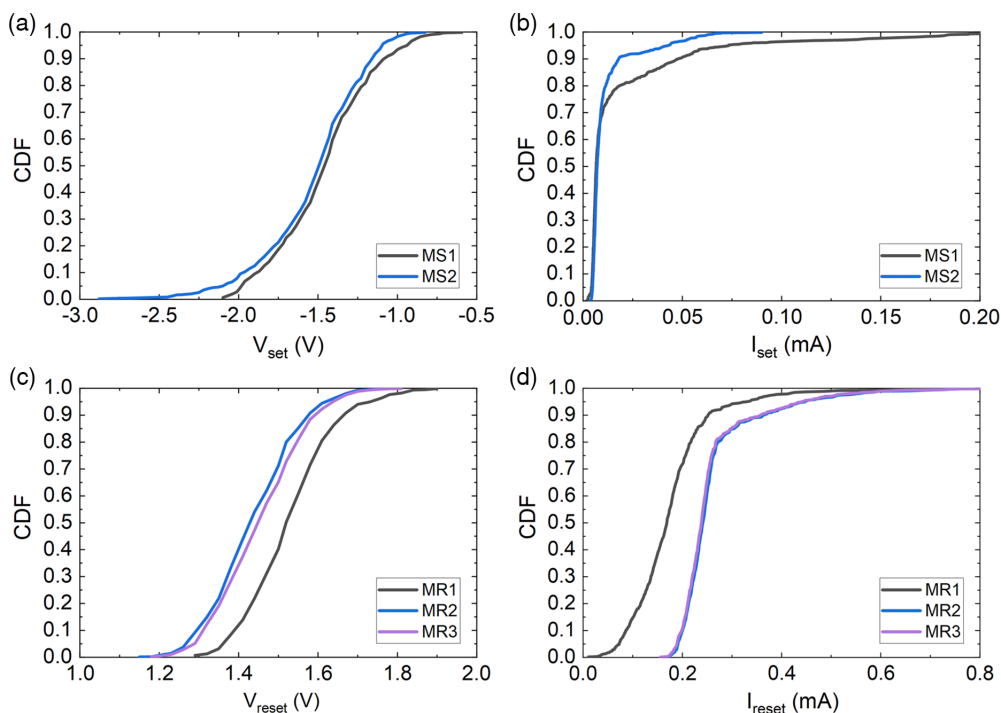


**Figure 9.** CDFs for a)  $V_{set}$ , b)  $I_{set}$ , c)  $V_{reset}$ , d)  $I_{reset}$ . The parameters are obtained with the different methods described above.

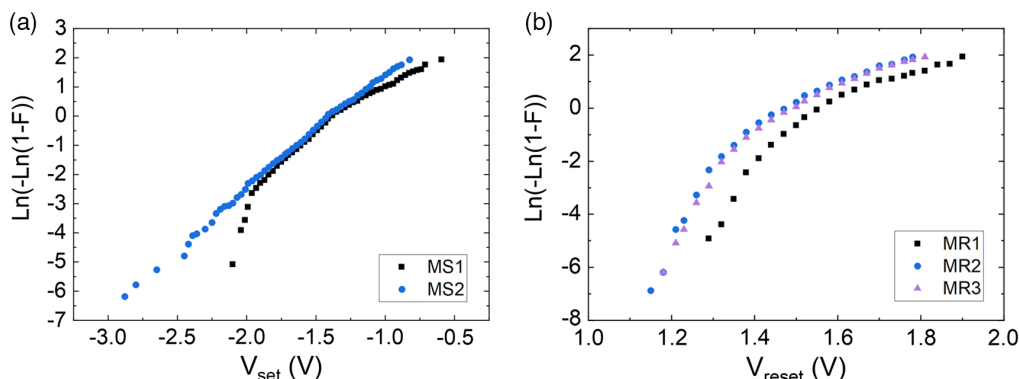


**Figure 10.** Weibulls for the RS parameters extracted with the different methods under consideration here are shown for a)  $V_{set}$  and b)  $V_{reset}$ . See that in most cases (save the  $V_{set}$  obtained with the MS2) the Weibull distribution function does not describe well the experimental data.

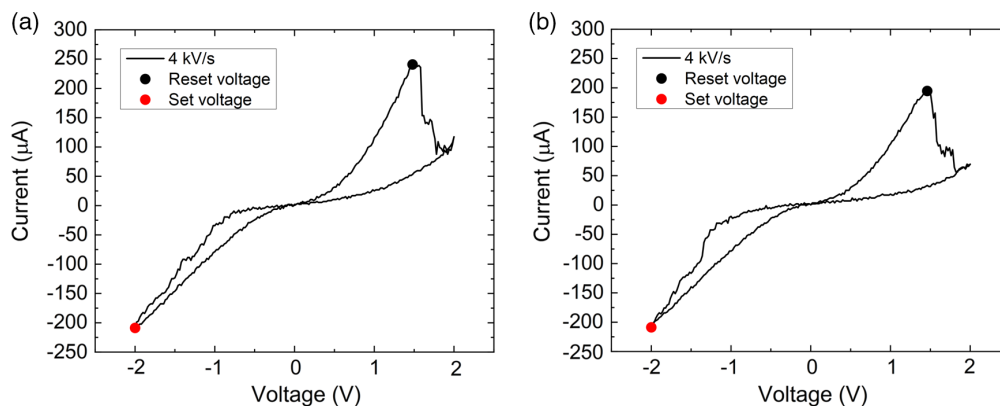


**Figure 11.**  $I$ - $V$  plots for the ramp rate  $4 \text{ kV s}^{-1}$ .

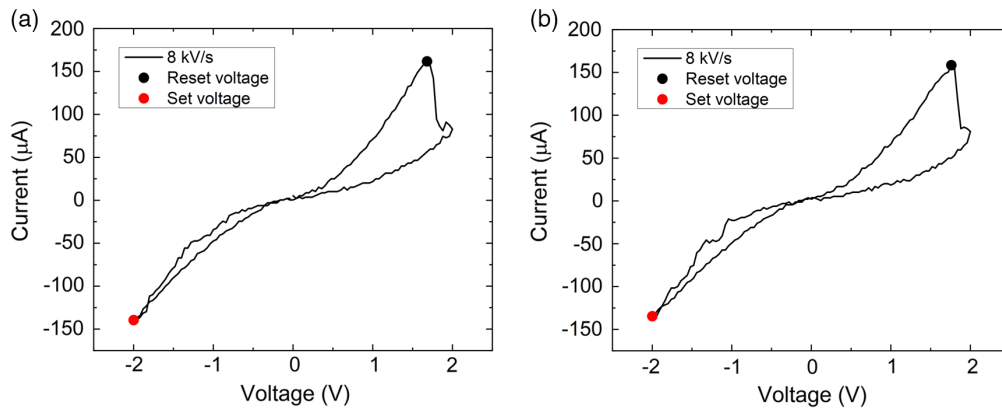


**Figure 12.**  $I$ - $V$  plots for the ramp rate  $8 \text{ kV s}^{-1}$ .

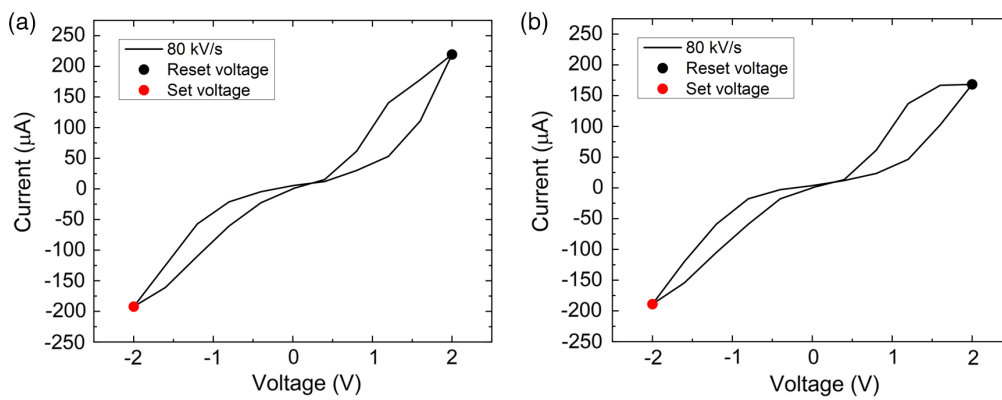


**Figure 13.**  $I$ - $V$  plots for the ramp rate  $80 \text{ kV s}^{-1}$ .

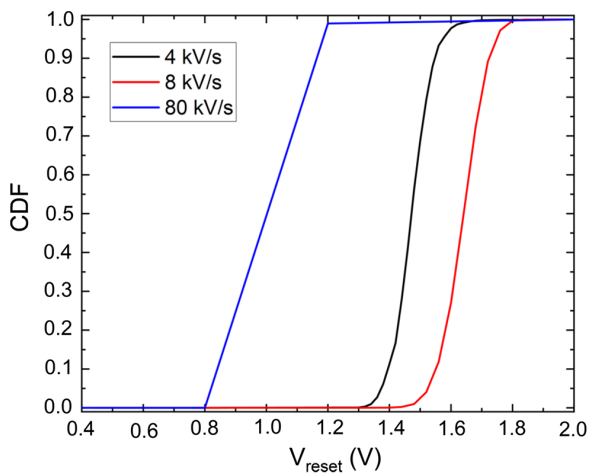


**Figure 14.** Reset voltage CDFs for different ramp rates.

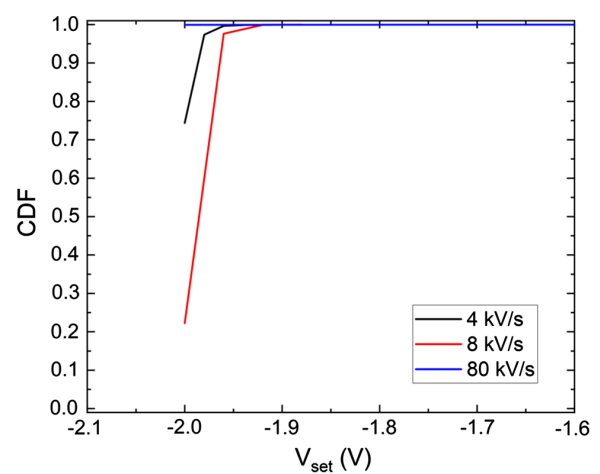


**Figure 15.** Set voltage CDFs for different ramp rates.

The  $V_{\text{set}}$  and  $V_{\text{reset}}$  for the cycles analyzed were obtained following the methodology described above. The CDFs are shown together in **Figure 14** and **15** to visualize the effects of the ramp rate.

It can be concluded from these data that the devices withstand a large number of switching cycles, which is about  $10^5$  for the

ramp rate of  $80 \text{ kV s}^{-1}$ . It should be noted that the corresponding cycling frequency coincides with that used in work<sup>[18]</sup> and significantly exceeds the frequencies used in other works, see, for example, other studies.<sup>[20,21]</sup> The extracted set voltages for the different frequencies are mostly the same due to the curves' shape.

In this respect, the maximum current (assuming absolute values) of the set cycles is almost always located at  $V = -2V$ . Nevertheless, this fact does not happen in the reset cycles, and multiple reset voltages could be extracted from the curves which resemble typical shapes for the lower ramp rates. For the ramp rates of 4 and  $8 \text{ kV s}^{-1}$ , the extracted values corresponding to  $V_{\text{reset}}$  reveal the tendency to increase with the frequency, according to the well-known time–voltage dilemma.<sup>[28]</sup> Namely, higher voltages are required for switching at higher sweep rate, especially for the larger switching times observed for reset transitions.<sup>[29]</sup> We should also take into account the high-voltage step for the highest cycling frequency corresponding to 0.4 V, which gives rise to the distorted shape of the  $I$ – $V$  curves and a low variability, underestimated due to the limited resolution of measurement circuit.

#### 4. Discussion

The results of RS measurements and their statistical analysis presented here allow selecting the appropriate parameter extraction techniques for the fabricated Au/Ta/ZrO<sub>2</sub>(Y)/Ta<sub>2</sub>O<sub>5</sub>/TiN/Ti memristive devices required for the simulation of higher-level memristive circuits with predictable variability. At the same time, the fabricated devices are quite large (20  $\mu\text{m}$  in size) and should be scaled down to a sub-micrometer level relevant for an application.<sup>[18]</sup> As the RS mechanism in metal–oxide devices fabricated by magnetron sputtering is multifilamentary in general, downscaling the technology could result in measurable changes in both RS parameters and their variability. In the considered devices, filaments form along boundaries of columnar grains with the lateral size of about 10 nm.<sup>[30]</sup> It is difficult to expect significant changes in D2D variability for the sub-micrometer-sized devices and uniform industrial technology. However, C2C variability considered in this article can change drastically with the decrease in device size due to the spatial constraints imposed on the filament ensemble.

Another issue considered in this article is the dependence of extracted parameters on the extraction methodology and on the measurement conditions. The extracted parameter values and their variability can be affected either by noise or insufficient resolution of measurement circuit. The latter factor becomes more significant with an increase in the cycling frequency, and its effect is superimposed on the basic regularities associated with the finite switching time, especially pronounced for the reset process.<sup>[29]</sup>

All these problems should be accurately addressed in further research and technology optimization with relevance to modern applications of memristors.

#### 5. Conclusions

Variability in Au/Ta/ZrO<sub>2</sub>(Y)/Ta<sub>2</sub>O<sub>5</sub>/TiN/Ti memristive devices has been studied under a statistical viewpoint. Herewith, different methods for extraction parameters of RS were established and assessed. The most representative RS parameters, such as  $V_{\text{set}}$ ,  $I_{\text{set}}$ ,  $V_{\text{reset}}$ , and  $I_{\text{reset}}$ , have been extracted and analyzed.

In particular, C2C variability is evaluated by determining the CDFs and the Weibits to determine the appropriateness of the

description using Weibull distribution. The extraction methods where the current derivative is involved led to a higher variability. The extraction results also depend on the sweep rate, although RS is found to be robust to high-frequency excitation. Lower variability is determined for the higher-frequency cycling due to the limited resolution of measurement circuit. Because of that, it has to be also considered that the results highly depend on the numerical method and on the measurement conditions employed, as demonstrated.

#### Acknowledgements

The authors acknowledge the Consejería de Conocimiento, Investigación y Universidad, Junta de Andalucía (Spain), European Regional Development Fund (ERDF) under projects A-TIC-117-UGR18, B-TIC-624-UGR20, and IE2017-5414. Support from the Government of the Russian Federation under Megagrant Program (agreement no. 074-02-2018-330 (2)) and the Ministry of Science and Higher Education of the Russian Federation under “Priority-2030” Academic Excellence Program of the Lobachevsky State University of Nizhny Novgorod (N-466-99\_2021-2023) is also acknowledged. Memristive devices were designed in the frame of the scientific program of the National Center for Physics and Mathematics (project “Artificial intelligence and big data in technical, industrial, natural and social systems”).

#### Conflict of Interest

The authors declare no conflict of interest.

#### Data Availability Statement

The data that support the findings of this study are available from the corresponding author upon reasonable request.

#### Keywords

memristors, resistive switching, resistive random access memory, tantalum oxide, variabilities, yttria-stabilized zirconia

Received: July 26, 2022

Revised: September 28, 2022

Published online:

- [1] Q. Xia, J. J. Yang, *Nat. Mater.* **2019**, *18*, 309.
- [2] *Memristors and Memristive Systems*, (Ed: R. Tetzlaff), Springer, New York, USA **2014**.
- [3] M. Lanza, A. Sebastian, W. D. Lu, M. Le Gallo, M.-F. Chang, D. Akinwande, F. M. Puglisi, H. N. Alshareef, M. Liu, J. B. Roldan, *Science* **2022**, *376*, abj9979.
- [4] A. Amirsoleimani, F. Alibart, V. Yon, J. Xu, M. R. Pazhouhandeh, S. Ecoffey, Y. Beilliard, R. Genov, D. Drouin, *Adv. Intell. Syst.* **2020**, *2*, 2000115.
- [5] M. Lanza, R. Waser, D. Ielmini, J. J. Yang, L. Goux, J. Suñe, A. J. Kenyon, A. Mehonic, S. Spiga, V. Rana, S. Wiefels, S. Menzel, I. Valov, M. A. Villena, E. Miranda, X. Jing, F. Campabadal, M. Gonzalez, F. Aguirre, F. Palumbo, K. Zhu, J. B. Roldan, F. M. Puglisi, L. Larcher, T.-H. Hou, T. Prodromakis, Y. Yang, P. Huang, T. Wang, Y. Chai, et al., *ACS Nano* **2021**, *15*, 17214.



- [6] Z. Wang, H. Wu, G. W. Burr, C. S. Hwang, K. L. Wang, Q. Xia, J. J. Yang, *Nat. Rev. Mater.* **2020**, *5*, 173.
- [7] M. Lanza, H.-S. P. Wong, E. Pop, D. Ielmini, D. Strukov, B. C. Regan, L. Larcher, M. A. Villena, J. J. Yang, L. Goux, A. Belmonte, Y. Yang, F. M. Puglisi, J. Kang, B. Magyari-Köpe, E. Yalon, A. Kenyon, M. Buckwell, A. Mehonic, A. Shluger, H. Li, T.-H. Hou, B. Hudec, D. Akinwande, R. Ge, S. Ambrogio, J. B. Roldan, E. Miranda, J. Suñe, K. L. Pey, et al., *Adv. Electron. Mater.* **2019**, *5*, 1800143.
- [8] A. N. Mikhaylov, D. V. Guseinov, A. I. Belov, D. S. Korolev, V. A. Shishmakova, M. N. Koryazhkina, D. O. Filatov, O. N. Gorshkov, D. Maldonado, F. J. Alonso, J. B. Roldán, A. V. Krichigin, N. V. Agudov, A. A. Dubkov, A. Carollo, B. Spagnolo, *Chaos Soliton. Fract.* **2021**, *144*, 110723.
- [9] M. Mishchenko, D. Bolshakov, V. Lukoyanov, D. Korolev, A. I. Belov, D. Guseinov, V. Matrosov, V. Kazantsev, A. N. Mikhaylov, *J. Phys. D: Appl. Phys.* **2022**, *55*, 394002.
- [10] A. Mikhaylov, A. Pimashkin, Y. Pigareva, S. Gerasimova, E. Gryaznov, S. Shchanikov, A. Zuev, M. Talanov, I. Lavrov, V. Demin, V. Erokhin, S. Lobov, I. Mukhina, V. Kazantsev, H. Wu, B. Spagnolo, *Front. Neurosci.* **2020**, *14*, 358.
- [11] V. Erokhin, *Bionanoscience* **2020**, *10*, 834.
- [12] R. Carboni, D. Ielmini, *Adv. Electron. Mater.* **2019**, *5*, 1900198.
- [13] V. J. Dowling, V. A. Slipko, Y. V. Pershin, *Chaos, Soliton. Fract.* **2021**, *142*, 110385.
- [14] B. Gao, B. Lin, Y. Pang, F. Xu, Y. Lu, Y.-C. Chiu, Z. Liu, J. Tang, M.-F. Chang, H. Qian, H. Wu, *Sci. Adv.* **2022**, *8*, eabn7753.
- [15] S. N. Danilin, S. A. Shchanikov, in *2015 IEEE Int. Conf. on Mechanical Engineering, Automation and Control Systems (MEACS)*, IEEE, Piscataway, NJ, USA **2015**, pp. 1–5.
- [16] S. N. Danilin, S. A. Shchanikov, A. E. Sakulin, I. A. Bordanov, in *2018 IEEE Conf. on Engineering and telecommunication (EnT-MIPT)*, IEEE, Piscataway, NJ, USA **2018**, pp. 205–209.
- [17] S. Shchanikov, A. Zuev, I. Bordanov, S. Danilin, V. Lukoyanov, D. Korolev, A. Belov, Y. Pigareva, A. Gladkov, A. Pimashkin, A. Mikhaylov, V. Kazantsev, A. Serb, *Chaos, Soliton. Fract.* **2021**, *142*, 110504.
- [18] T. Hennen, A. Elias, J.-F. Nodin, G. Molas, R. Waser, D. J. Wouters, D. Bedau, *Front. Neurosci.* **2022**, *16*, 941753.
- [19] D. A. Zhevnenko, F. P. Meshchaninov, V. S. Kozhevnikov, E. S. Shamin, O. A. Telminov, E. S. Gornev, *Micromachines* **2021**, *12*, 1220.
- [20] B. Garda, *Energies* **2021**, *14*, 7264.
- [21] V. Ostrovskii, P. Fedoseev, Y. Bobrova, D. Butusov, *Nanomaterials* **2022**, *12*, 63.
- [22] J. B. Roldan, D. Maldonado, C. Aguilera-Pedregosa, F. J. Alonso, Y. Xiao, Y. Shen, W. Zheng, Y. Yuan, M. Lanza, in *Modeling the Variability of Au/Ti/h-BN/Au Memristive Devices*, IEEE, Piscataway, NJ, USA **2022**, p. 1.
- [23] D. Zhevnenko, F. Meshchaninov, V. Kozhevnikov, E. Shamin, A. Belov, S. Gerasimova, D. Guseinov, A. Mikhaylov, E. Gornev, *Chaos Soliton. Fract.* **2021**, *142*, 110382.
- [24] A. Mikhaylov, A. Belov, D. Korolev, I. Antonov, V. Kotomina, A. Kotina, E. Gryaznov, A. Sharapov, M. Koryazhkina, R. Kryukov, S. Zubkov, A. Sushkov, D. Pavlov, S. Tikhov, O. Morozov, D. Tetelbaum, *Adv. Mater. Technol.* **2020**, *5*, 1900607.
- [25] E. Pérez, D. Maldonado, C. Acal, J. E. Ruiz-Castro, F. J. Alonso, A. M. Aguilera, F. Jiménez-Molinos, Ch. Wenger, J. B. Roldán, *Microelectron. Eng.* **2019**, *214*, 104.
- [26] J. B. Roldán, F. J. Alonso, A. M. Aguilera, D. Maldonado, M. Lanza, *J. Appl. Phys.* **2019**, *125*, 174504.
- [27] D. Maldonado, S. Aldana, M. B. González, F. Jiménez-Molinos, M. J. Ibáñez, D. Barrera, F. Campabadal, J. B. Roldán, *Microelectron. Eng.* **2022**, *257*, 111736.
- [28] S. Menzel, U. Böttger, M. Wimmer, M. Salinga, *Adv. Funct. Mater.* **2015**, *25*, 6306.
- [29] M. Csontos, Y. Horst, N. J. Olalla, U. Koch, I. Shorubalko, A. Halbritter, J. Leuthold, Picosecond Time-Scale Resistive Switching Monitored in Real-Time, arXiv:2209.06732v1, **2022**.
- [30] A. N. Mikhaylov, E. G. Gryaznov, A. I. Belov, D. S. Korolev, A. N. Sharapov, D. V. Guseinov, D. I. Tetelbaum, S. V. Tikhov, N. V. Malekhonova, A. I. Bobrov, D. A. Pavlov, S. A. Gerasimova, V. B. Kazantsev, N. V. Agudov, A. A. Dubkov, C. M. M. Rosário, N. A. Sobolev, B. Spagnolo, *Phys. Status Solidi C* **2016**, *13*, 870.